The retromer component sorting nexin-1 is required for efficient retrograde transport of Shiga toxin from early endosome to the trans Golgi network

Miriam V. Bujny[1], Vincent Popoff[2], Ludger Johannes[2,*] and Peter J. Cullen[1,*]

[1]The Henry Wellcome Integrated Signalling Laboratories, Department of Biochemistry, School of Medical Sciences, University of Bristol, Bristol, BS8 1TD, UK

[2]Traffic and Signaling Laboratory, UMR144 Curie/Centre National de la Recherche Scientifique, Institut Curie, Paris, France

*Authors for correspondence (e-mails: Ludger.Johannes@curie.fr; Pete.Cullen@bris.ac.uk)

Accepted 20 April 2007
Journal of Cell Science 120, 2010-2021 Published by The Company of Biologists 2007
doi:10.1242/jcs.003111

Summary

The mammalian retromer complex is a multi-protein complex that regulates retrograde transport of the cation-independent mannose 6-phosphate receptor (CI-MPR) from early endosomes to the trans Golgi network (TGN). It consists of two subcomplexes: a membrane-bound coat comprising sorting nexin-1 (SNX1) and possibly sorting nexin-2 (SNX2), and a cargo-selective subcomplex, composed of VPS26, VPS29 and VPS35. In addition to the retromer, a variety of other protein complexes has been suggested to regulate endosome-to-TGN transport of not only the CI-MPR but a wide range of other cargo proteins. Here, we have examined the role of SNX1 and SNX2 in endosomal sorting of Shiga and cholera toxins, two toxins that undergo endosome-to-TGN transport en route to their cellular targets located within the cytosol. By using small interfering RNA (siRNA)-mediated silencing combined with single-cell fluorescent-toxin-uptake assays and well-established biochemical assays to analyze toxin delivery to the TGN, we have established that suppression of SNX1 leads to a significant reduction in the efficiency of endosome-to-TGN transport of the Shiga toxin B-subunit. Furthermore, we show that for the B subunit of cholera toxin, retrograde endosome-to-TGN transport is less reliant upon SNX1. Overall, our data establish a role for SNX1 in the endosome-to-TGN transport of Shiga toxin and are indicative for a fundamental difference between endosomal sorting of Shiga and cholera toxins into endosome-to-TGN retrograde transport pathways.

Key words: SNX1, SNX2, Retromer, Shiga toxin, Cholera toxin, Retrograde transport

Introduction

The retromer complex was originally identified in yeast where it regulates retrograde endosome-to-Golgi transport of the vacuolar protein sorting receptor Vps10p (Seaman et al., 1997; Seaman et al., 1998). This multi-protein complex consists of two subcomplexes. One subcomplex comprises the sorting nexins Vps5p and Vps17p, which form a membrane-bound coat (Seaman et al., 1998; Seaman and Williams, 2002). The second subcomplex is composed of Vps26p, Vps29p and Vps35p (Seaman et al., 1997; Reddy and Seaman, 2001), and is cargo-selective because Vps35p associates with the cytosolic region of Vps10p (Nothwehr et al., 2000; Burda et al., 2002). The retromer complex is highly conserved, and homologs have been identified in a number of organisms, including *S. pombe*, *C. elegans*, *Drosophila*, plants and mammals, suggesting a fundamental and conserved function for this complex in retrograde transport (Kurten et al., 1996; Haft et al., 2000; Iwaki et al., 2006; Jaillais et al., 2006; Oliviusson et al., 2006; Prasad and Clark, 2006; Shimada et al., 2006) and reviewed in Seaman (Seaman, 2005).

For the mammalian retromer complex, homologs of all yeast proteins have been identified, with the possible exception of Vps17p (Haft et al., 2000). A recent study identified the cation-independent mannose 6-phosphate receptor (CI-MPR) as cargo for the retromer, because it directly binds to VPS35 (Arighi et al., 2004). Independent studies have established that small interfering RNA (siRNA)-mediated suppression of not only individual components of the VPS26-VPS29-VPS35 subcomplex, but also the Vps5p homolog sorting nexin-1 (SNX1) perturbs retrograde endosome-to-TGN transport of the CI-MPR (Arighi et al., 2004; Seaman, 2004; Carlton et al., 2004). In mammalian cells, the CI-MPR performs an equivalent role to yeast Vps10p in the transport of lysosomal hydrolases and, thus, such data argue for an evolutionarily conserved role of the retromer in regulating retrograde endosome-to-Golgi transport.

In addition to the retromer, a variety of other proteins appears to play important roles in retrograde endosome-to-TGN transport. This includes phosphofurin acidic-cluster-sorting protein 1 (PACS1), a protein that has been shown to mediate endosome-to-TGN retrieval of the CI-MPR by forming a complex with the clathrin adaptors AP1 and GGA3, and also casein kinase 2 (Wan et al., 1998; Meyer et al., 2000; Crump et al., 2001; Scott et al., 2003; Scott et al., 2006). Furthermore, a Rab9-TIP47 complex has been shown to regulate retrieval of the CI-MPR from late endosomes to the Golgi complex (Lombardi et al., 1993; Diaz and Pfeffer, 1998; Carroll et al., 2001). The presence of such distinct sorting

complexes underscores the high complexity and need for tight regulation of the endosome-to-TGN itinerary as, indeed, in addition to the CI-MPR, a wide range of other cargo molecules are transported on this retrograde itinerary (Bonifacino and Rojas, 2006). This range includes transmembrane proteins such as sortilin, TGN38/46 and furin and, of particular relevance for the present study, the bacterial exotoxins produced by *Shigella dysenteriae* and *Vibrio cholerae* (Shiga toxin and cholera toxin, respectively).

Shiga and cholera toxins are both AB_5-type toxins, consisting of an enzymatically active A subunit, and a pentamer of B subunits that directs the association of the toxin with the cell surface (Sandvig and van Deurs, 2005; Johannes and Decaudin, 2005). In case of Shiga toxin, the B subunits bind to the glycosphingolipid globotriaosylceramide (Gb3) (Jacewicz et al., 1986), whereas the cholera toxin B subunits show high affinity for the ganglioside GM1 (Fishman et al., 1976). Once associated with their respective cell-surface receptors, each toxin is endocytosed via clathrin-dependent and -independent mechanisms (Sandvig and van Deurs, 2002; Sandvig and van Deurs, 2005). Following internalization into the endosomal network, the respective toxin bypasses recycling and degradative pathways (Mallard et al., 1998) and undergoes retrograde transport, initially from endosomes into the Golgi complex and then on to the endoplasmic reticulum before finally being retro-translocated into the cytosol (Sandvig and van Deurs, 2005; Spooner et al., 2006).

In the case of Shiga toxin, retrograde endosome-to-TGN transport appears to require a multitude of structural and coat proteins, including clathrin and its adaptor epsinR (Lauvrak et al., 2004; Saint-Pol et al., 2004), the large GTPase dynamin (Lauvrak et al., 2004) and Rab6A′ (Mallard et al., 2002; Del Nery et al., 2006). Furthermore, components of the fusion machinery on the TGN side, including golgin-97 and tGolgin-1 (Lu et al., 2004; Yoshino et al., 2005), and two different SNARE complexes containing syntaxin 5 and syntaxin 16 (Mallard et al., 2002; Tai et al., 2004; Amessou et al., 2007) have been shown to be essential. By contrast, retrograde transport of cholera toxin is less well understood, although it has been proposed that both toxins enter the Golgi complex via the same transport intermediates (Nichols et al., 2001).

With an emerging role for the retromer in endosome-to-TGN transport, an important question is how this pathway relates to other, paralleled endosome-to-TGN retrograde itineraries. In this study, we have begun to address this question by examining the role of SNX1 and sorting nexin-2 (SNX2), a proposed functional analog of Vps17p, in retrograde transport of Shiga and cholera toxin. By using siRNA-mediated silencing combined with single-cell fluorescent-toxin-uptake assays and well-established biochemical assays to analyze toxin delivery to the TGN, we present data that establishes a role of SNX1 in endosome-to-TGN transport of Shiga toxin B-subunit, whereas, in our assays, involvement of SNX2 was a less prominent. In addition, we show that the retrograde transport of cholera toxin B-subunit is less reliant upon SNX1. These results clearly highlight the existence of a fundamental difference between the sorting mechanisms for Shiga toxin compared with those for cholera toxin into this retrograde pathway.

Results

Following endocytosis, Shiga toxin is transported via SNX1-labeled early endosomes to the TGN

Previous work has established that endogenous SNX1 preferentially associates with highly curved membrane surfaces of early endosomes. This association is mediated through the combined action of its phosphatidylinositol-3-monophosphate-binding phagocyte oxidase (phox) homology (PX) domain and its C-terminal Bin-amphiphysin-Rvs (BAR) domain (Carlton et al., 2004). To examine whether internalized Shiga toxin was transported through the SNX1-positive early endosome to the TGN, we performed an immunofluorescence-based toxin-uptake assay. For this, HeLa cells were surface-labeled with FITC-conjugated Shiga toxin B-subunit (FITC-STxB) at 4°C. After extensive washes to remove all unbound toxin, cells were warmed to 37°C and fixed at various time points before visualizing the degree of colocalization with endogenous SNX1 by immunofluorescence labeling. This assay revealed that the toxin initially had labeled the cell surface and then, after 10 minutes, underwent internalization (Fig. 1A,B). The FITC-STxB punctae colocalized well with SNX1-positive peripheral vesicular and tubular profiles, but especially with SNX1-labeled structures in the juxtanuclear area (Fig. 1B). We noticed that although most (69.1%) SNX1-positive structures were FITC-STxB-positive (481 structures out of 696 SNX1-positive vesicles for the example shown), only 33.3% of all FITC-STxB punctae were SNX1-positive (481 out of 1445). When incubated at 19.5°C for 1 hour, the toxin could be ‘trapped’ successfully in SNX1-positive structures (Fig. 1C), because incubation at this temperature still allows for successful internalization into endosomes but has been shown to block endosome-to-TGN trafficking of the toxin (Mallard et al., 1998). Again, not all (40%) STxB-positive structures were labeled for SNX1 (851 out of 2100 FITC-STxB-decorated structures positive for SNX1). Under these non-permissive conditions, markedly fewer cells showed the previously observed clustering of SNX1-positive endosomes at the juxtanuclear area. Under permissive conditions (37°C), the degree of colocalization with SNX1 on more peripheral punctae decreased with time (Fig. 1D-F), whereas SNX1-labeled structures in the perinuclear area still colocalized with the toxin. At these time points, FITC-STxB became progressively enriched in the juxtanuclear area where it colocalized with TGN46, a well-established marker protein of the TGN (Fig. 1F). Taken together, these data establish that, after internalization, the Shiga toxin B-subunit is partially delivered to and transported via SNX1-positive early endosomes prior to its enrichment at the TGN.

Suppression of SNX1 by RNA interference perturbs retrograde early-endosome-to-TGN transport of Shiga toxin B-subunit

To define the function of SNX1 in early endosome-to-TGN transport of Shiga toxin, we employed RNA interference (RNAi) to suppress expression of SNX1 using a previously characterized SNX1-specific siRNA (Carlton et al., 2004) and again performed the previously described immunofluorescence toxin-uptake experiments. Importantly, we found that FITC-STxB labeled the cell surface in SNX1-suppressed HeLa cells to the same extent as in control cells (Fig. 2A). However, in stark contrast to control cells, where the toxin began to display

enrichment at the juxtanuclear region after 30 minutes, in SNX1-suppressed cells the toxin remained predominantly associated with more peripheral structures (Fig. 2B). This difference in Shiga toxin transport was even more evident when examined at later time points. After a 60-minute incubation, the toxin displayed a compact juxtanuclear accumulation at the TGN in control cells, whereas in SNX1-suppressed cells – even after 120 minutes – FITC-STxB exhibited still a more dispersed peripheral localization, with only slight perinuclear enrichment (Fig. 2C,D).

To quantify these data, we initially employed a strategy where we inspected the localization of FITC-STxB in individual cells within a population and scored the frequency at which we observed the appearance of two distinct morphologies, being either a tight TGN-like juxtanuclear stain or a more dispersed peripheral appearance (Fig. 3A,B). This type of 'analog analysis' revealed that, after 30 minutes, 55% of control cells showed a clear TGN-like enrichment of the STxB, whereas only 33% of SNX1-suppressed cells displayed this phenotype (Fig. 3C). To further examine the effect of SNX1 on the kinetics of STxB delivery to the TGN, we extended this analysis by scoring the FITC-STxB distribution in control and SNX1-suppressed cells over time (Fig. 3D). Using this approach, we confirmed that in SNX1-suppressed cells, the rate of enrichment of STxB in the perinuclear area was markedly reduced when compared with control cells.

To quantify these findings further, we also analyzed the degree of colocalization between internalized FITC-STxB and TGN46 (a known TGN marker protein) with a digital analysis approach using MetaMorph software (Fig. 3E). This method confirmed that, after 30 minutes internalization, accumulation of STxB at the TGN-Golgi complex was markedly reduced in SNX1-suppressed cells (12% ± 1% standard deviation) when compared with control cells (37±0.4%). Importantly, as previously reported (Carlton et al., 2004), SNX1-suppression did not appear to grossly perturb the integrity of the TGN or the Golgi complex as judged by light microscopy when immunolabeling with anti-giantin or anti-TGN46 antibodies (Fig. 4A,B). Overall, these data are therefore consistent with a model in which SNX1 is required for the efficient transport of Shiga toxin between the early endosome and the TGN, in a manner where – under conditions of SNX1-suppression – the rate of endosome-to-TGN transport of the toxin is markedly reduced.

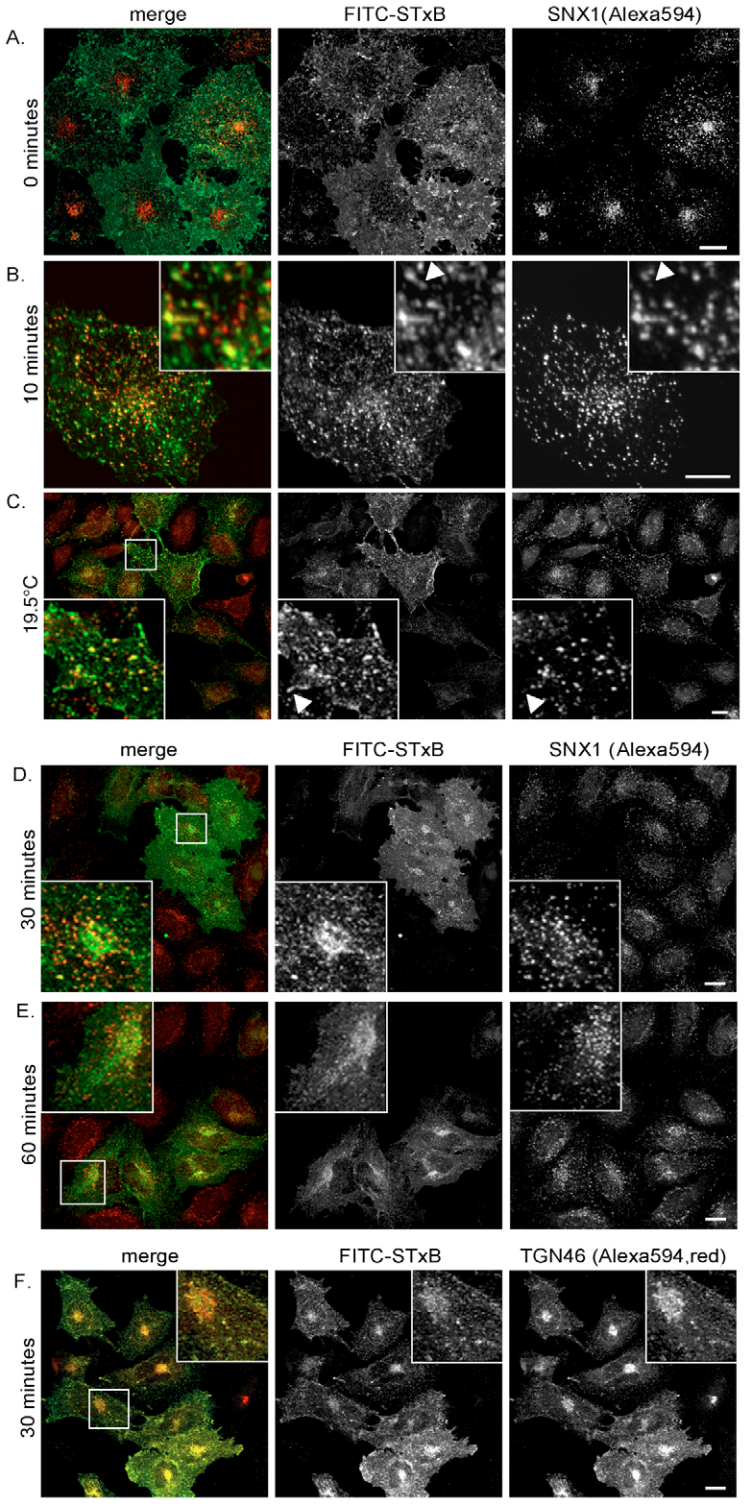

Fig. 1. Shiga toxin B-subunit is transported via SNX1-positive endosomes to the TGN. Fluorescence-labeled Shiga toxin B-subunit (FITC-STxB, green channel) was surface-bound to HeLa cells at 4°C and subsequently allowed to internalize for the indicated times at 37°C or 19.5°C; cells were fixed and immunolabeled for endogenous SNX1 (Alexa594, red channel) and imaged using confocal microscopy. Maximum projections of eight to ten optical *z*-slices (480 nm *z*-separation) are shown. (A) Cells were fixed without incubation at 37°C (0 minutes). (B) After 10 minutes at 37°C, the Shiga toxin B-subunit extensively colocalized with the SNX1-positive endosomal structures (yellow color in merged images). Note the subset of FITC-STxB tubules negative for SNX1 (arrowheads in B and C). (C) Shiga toxin B-subunit accumulated in SNX1-positive endosomes when incubated at 19.5°C for 1 hour. When incubated for longer times at 37°C (D,E), it displayed a TGN-like enrichment at the juxtanuclear area. (F) At these time points, Shiga toxin B-subunit colocalised extensively with TGN46 (Alexa594, red). Bars, 10 μm.

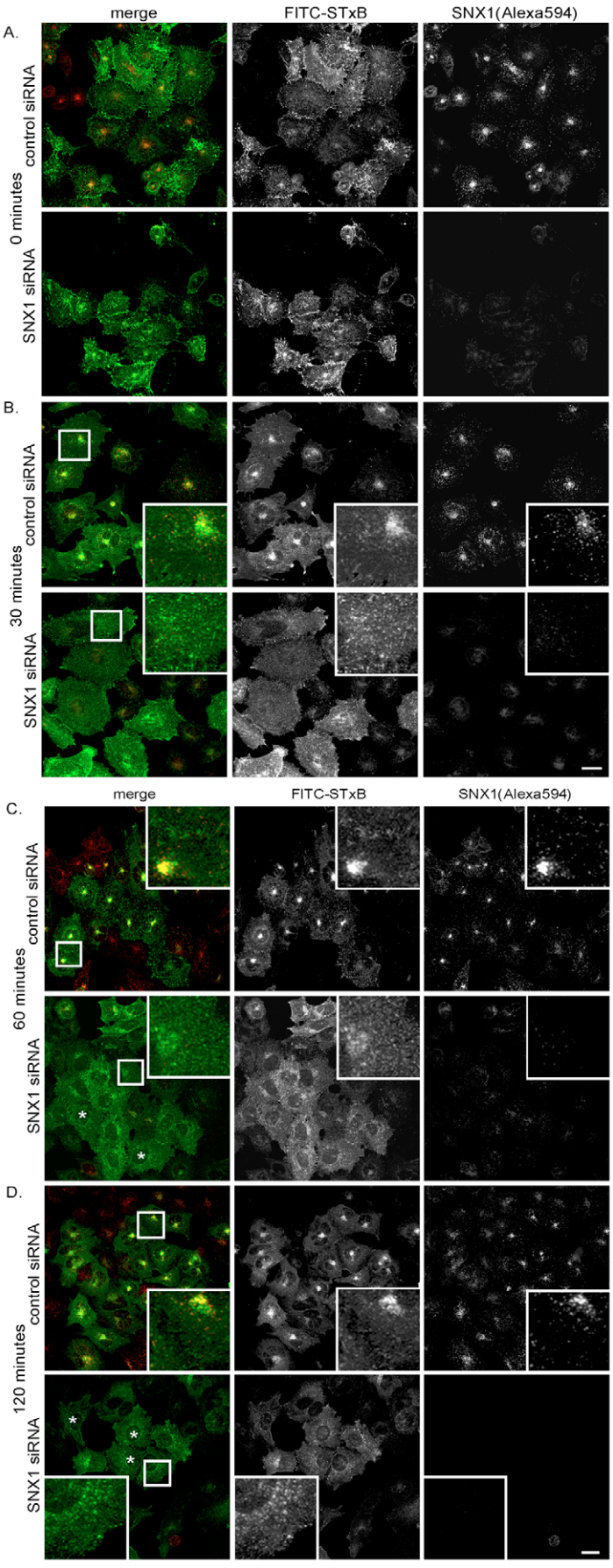

Fig. 2. In SNX1-suppressed cells, retrograde endosome-to-TGN transport of FITC-STxB is markedly perturbed. HeLa cells were treated with either control or SNX1-specific siRNA. After 72 hours, toxin uptake assays using FITX-STxB (green channel) were performed. Cells were fixed at indicated times and immunolabeled for SNX1 (Alexa594, red channel). In cells treated with SNX1-specific siRNA, the immunofluorescence signal was markedly reduced. (A) When cells were fixed without prior incubation at 37°C, the toxin was found to label the plasma membrane to comparable levels in control and SNX1-suppressed conditions. (B) After 30 minutes of internalization, the toxin showed juxtanuclear enrichment in control siRNA-treated cells, but remained associated with more peripheral structures in SNX1-suppressed cells. Even after 60 minutes (C) and 120 minutes (D), only moderate amounts of the toxin had reached the TGN area in SNX1-suppressed cells with most cells still displaying vesicular enrichment of the toxin (asterisks). Bars, 20 μm.

A biochemical analysis confirms the requirement for SNX1 in endosome-to-TGN transport of Shiga toxin

As is has been reported that certain toxins might traffic through a compartment without ever being visible due to their high exit rate (Sandvig and van Deurs, 2002), we sought to confirm our findings by a non-microscopy-based approach. We thus resorted to a well-established, biochemical assay that can also account for the observed cell-to-cell variability regarding the amounts of internalized toxin per individual cell. Here, we made use of a modified Shiga toxin B-subunit [B-($Sulf_2$)] that has been genetically engineered to contain a tandem tyrosine sulfation site while maintaining its transport itinerary (Mallard et al., 1998). Since protein sulfation only occurs in the TGN (Niehrs and Huttner, 1990), this modified toxin subunit allows the quantification of the kinetics of initial toxin arrival at this organelle. Thus, by providing cells with a source of radioactively labeled sulfate and measuring the incorporation of [^{35}S]-sulfate into the modified Shiga toxin B-subunit, the degree of toxin sulfation serves as a direct readout for TGN arrival.

For each assay, we assessed the levels of SNX1 protein in whole-cell lysates after treatment with control and SNX1-specific siRNA by western blotting (Fig. 5A), confirming successful suppression of protein expression in the entire cell population. Cells from the same batch were subsequently used for sulfation assays, in which the sulfate-starved cells were surface-labeled with the modified toxin subunit B-($Sulf_2$) at 4°C. After extensive washes, cells were incubated for 20 minutes at 37°C in pre-warmed growth medium containing radiolabeled sulfate and subsequently lyzed. The toxin was immunoprecipitated and the degree of its sulfation was monitored by autoradiography (see Materials and Methods for details). This analysis showed that, compared with control cells, the degree of sulfation was clearly decreased in SNX1-suppressed cells (Fig. 5B, inset). Quantification of band intensities using densitometry of six independent experiments (each in duplicate) revealed that sulfation of the modified toxin was reduced to 57±24.4% in SNX1-suppressed cells (Fig. 5B) after normalization for overall protein sulfation (see Materials and Methods). As we noticed that in some instances even comparably high levels of SNX1 suppression did not appear to inhibit STxB

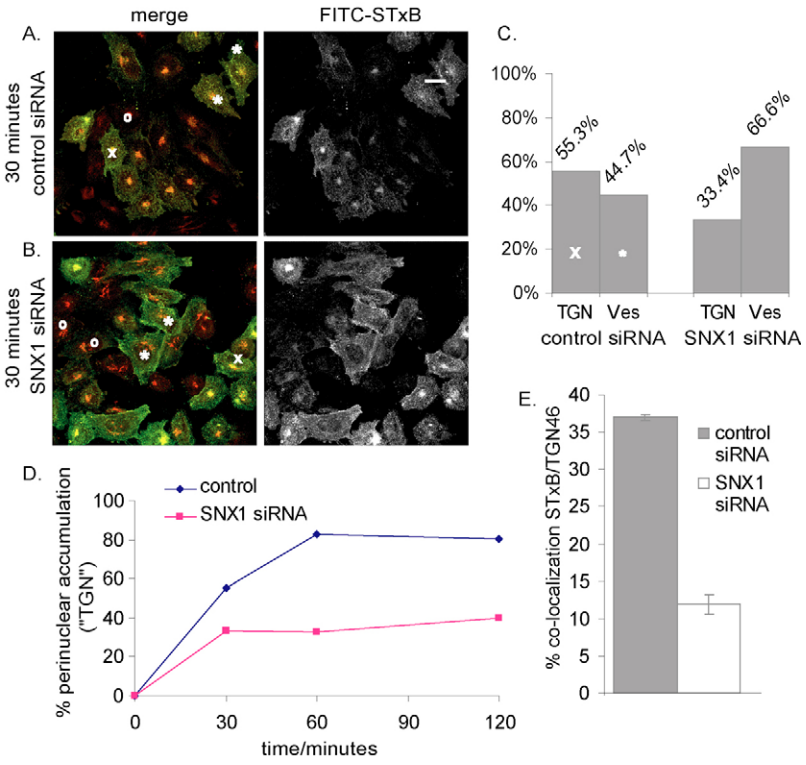

Fig. 3. Quantification of the defect in endosome-to-TGN transport in SNX1-suppressed cells. Toxin-uptake assays using control and SNX1-suppressed HeLa cells were performed as described. After fixation and immunolabeling with anti-SNX1 (Alexa594, red channel), samples were inspected by epifluorescence microscopy and scored blindly for either a TGN-like enrichment (×) or a vesicular appearance (*). Cells marked 'o' were not scored because of low toxin levels. (A,B) Scoring phenotypes; FITC-STxB in green channel and TGN46 (Alexa594) in red channel for control and SNX1-suppressed cells after 30 minutes of uptake. (C) Representative data for a set of control and SNX1-suppressed cells (n>600) after 30 minutes of toxin uptake. (D) TGN-like accumulation of FITC-STxB over time (n>600 for each sample; scored for 30, 60 and 120 minutes) for SNX1-suppressed and control cells. (E) Colocalization of FITC-STxB and TGN46, digitally quantified from confocal images using MetaMorph software (see Materials and Methods for details). In control cells, 37±0.4% of FITC-STxB colocalized with TGN46 after 30 minutes of internalization, whereas SNX1-suppressed cells showed 12±1% colocalization. Values given are ± the standard deviation and were determined from the mean of individual visual fields for a total of n>50 cells. Bar, 20 μm.

sulfation or result in CI-MPR redistribution, we sought to determine to what extent the level of suppression influences the retrograde transport. In an attempt to correlate suppression efficiency with the sulfation state of B-($Sulf_2$), we plotted the achieved levels of siRNA-mediated suppression of each individual experimental set (x-axis) against the corresponding levels of B-($Sulf_2$) sulfation (y-axis) (Fig. 5C). From this analysis we concluded that, only suppression levels of SNX1 greater than 92% resulted in a marked sulfation inhibition (46.3±13.05% for these four sets, each in duplicates) whereas lower levels (<89%) did not lead to a clear reduction in B-($Sulf_2$) sulfation (Fig. 5C, asterisk). These data of decreased sulfation under SNX1-suppressed conditions are consistent with a reduced rate of Shiga-toxin-B-subunit delivery to the TGN from early endosomes and, hence, independently confirm the conclusions reached from the immunofluorescence studies. Further still, they point towards a minimal but crucial level of SNX1 to maintain efficient endosome-to-TGN transport.

As part of the biochemical characterization, we also examined the effect of SNX2 suppression on STxB sulfation. SNX2 is a protein that is highly related to SNX1, and our reasoning behind including this sorting nexin stemmed from the ongoing debate surrounding whether or not SNX2 is a functional component of the mammalian retromer complex (see Carlton et al., 2005; Rojas et al., 2007). Using a previously characterized siRNA (Carlton et al., 2005), we successfully suppressed SNX2 protein expression, as assessed by western blotting (Fig. 5A). In the sulfation assays, this reduction of SNX2 resulted in a minor reduction in toxin sulfation (78±26.7%) that was noticeable less compared with the strong effect of SNX1 suppression on B-($Sulf_2$) sulfation (Fig. 5B,C). Importantly, when looking at each individual experimental data set, the level of B-($Sulf_2$) sulfation under SNX2-suppressed conditions always exceeded the sulfation levels obtained for SNX1-suppressed (data not shown). The generally lower suppression levels obtained for SNX2-suppression resulted in a small inhibition in sulfation; however; even suppression greater than 91% did not subsantially inhibit sulfation (Fig. 5C). We furthermore noticed that SNX2-suppressed cells but not SNX1-suppressed cells proliferated less efficiently; we compensated this by counting and reseeding the cells a day before the assay (see Materials and Methods). As lower cell numbers would make interpretation of the biochemical data problematic, and given that overall protein sulfation was slightly more reduced in SNX2-suppressed cells (Fig. 5D), we sought to additionally investigate the effect of SNX2-suppression on STxB transport at single-cell level.

Analogous to the results obtained for SNX1, one would interpret the minor decrease in STxB sulfation observed in SNX2-suppressed cells as indicative for reduced toxin arrival at the TGN and, thus, expect a dispersed FITC-STxB pattern in immunofluorescent-toxin-uptake assays. Yet, we found that the localization of internalized FITC-STxB was not markedly altered. In SNX2-suppressed cells, after 30 minutes of internalization, the FITC-STxB showed a clear TGN-like enrichment (Fig. 6A) that was comparable with the degree of enrichment observed in control cells (Fig. 2A). This juxtanuclear accumulation of FITC-STxB colocalized well with TGN46 (Fig. 6B) and a detailed colocalization analysis of this data showed that the degree of TGN-enrichment of the toxin was not significantly altered in SNX2-suppressed cells (40±8%), when compared with control cells (37±0.4%) (Fig. 6C). Furthermore, when we analyzed the kinetics of toxin transport scoring the frequency of the previously characterized two distinct morphologies (Fig. 3A,B), we could not distinguish between control and SNX2-suppressed samples

(Fig. 7A,B). From this type of single-cell analysis, which is independent of absolute cell numbers in the sample, we thus conclude that SNX2-suppression does not lead to marked retention of STxB in endosomal structures en route to the TGN.

Concerning retrograde transport of endogenous receptors, a more recent study suggested that SNX1 and SNX2 have essential but interchangeable functions in endosome-to-TGN transport of the CI-MPR (Rojas et al., 2007). By contrast, we found here that STxB transport to the TGN appeared less reliant upon SNX2 and we thus sought to investigate toxin transport under conditions where both SNXs are jointly suppressed. Under these conditions, one would expect to see at least the phenotype observed in SNX1 depleted cells, as suppression of this sorting nexin produced a striking phenotype in all assays. Indeed, when we analyzed the distribution of FITC-STxB by fluorescent-toxin-uptake assays in jointly suppressed cells, we found that the toxin predominantly displayed a vesicular distribution (Fig. 7A), which was indistinguishable to the localization observed in SNX1-supressed cells (Fig. 3C). Importantly, when we analyzed the kinetics of toxin transport scoring the frequency of the previously characterized two distinct morphologies (Fig. 3A,B), we could not discriminate between the jointly SNX1- and SNX2-suppressed cells, and SNX1-suppressed samples (Fig. 7B). This finding corroborates a model in which SNX1 suppression, alone or in combination with SNX2, results in the vesicular retention of STxB. Concordantly, in cells in which SNX1 is suppressed, SNX2 appears more dispersed compared with control cells after 30 minutes of FITC-STxB uptake (Fig. 7C). Further still, SNX1 displays equally compact juxtanuclear enrichment in control and SNX2-suppressed cells (Fig. 6A). Overall, these data are consistent with the conclusion that SNX1 is required for efficient endosome-to-TGN transport because its suppression leads to a marked reduction of endosome-to-TGN transport of STxB and its retention in an endosomal compartment. SNX2 appears to be less important in promoting the endosome-to-TGN transport step of STxB, at least under these experimental conditions. Although the results from the single-cell analysis for jointly SNX1- and SNX2-suppressed cells were striking, for completeness, we sought to complement these data by a sulfation study. Interpretation of the results was, however, difficult because under these conditions global sulfation was affected.

In contrast to Shiga toxin, suppression of SNX1 does not affect cholera toxin endosome-to-TGN retrograde transport

Compared with Shiga toxin, relatively little is known about the endosome-to-TGN transport machinery involved in retrograde traffic of cholera toxin. It is has previously been suggested that both toxins enter the TGN via the same transport intermediates (Nichols et al., 2001). Thus, we sought to examine whether SNX1, besides affecting STxB transport, also plays a role in the retrograde transport of cholera toxin. We thus adapted the previously described immunofluorescence toxin-uptake assays to study cholera toxin traffic, employing cholera toxin B subunit coupled to Alexa Fluor-555 (Alexa^{555}-CTxB).

When Alexa^{555}-CTxB was surface-bound to control and SNX1-suppressed cells, it labeled the plasma membrane to the same extend (Fig. 8A). However, we noticed that the degree of fluorescence labeling was similarly heterogeneous for both conditions and that not all cells appeared to bind to Alexa^{555}-CTxB. After internalization for 15 minutes, Alexa^{555}-CTxB showed extensive colocalization with SNX1-positive early endosomes in control cells, and displayed a comparable punctate distribution in SNX1-suppressed HeLa cells (Fig. 8B). Like in cells treated with FITC-STxB, we noticed a strong accumulation of SNX1 in the perinuclear area in control cells. With time, Alexa^{555}-CTxB became progressively enriched in the perinuclear area (Fig. 8C,D). In stark contrast to the punctuate distribution of FITC-STxB (Fig. 2B,C) the Alexa^{555}-CTxB label displayed a juxtanuclear enrichment in the perinuclear area of SNX1-suppressed cells, which was comparable to the distribution of toxin B-subunit in control RNAi-

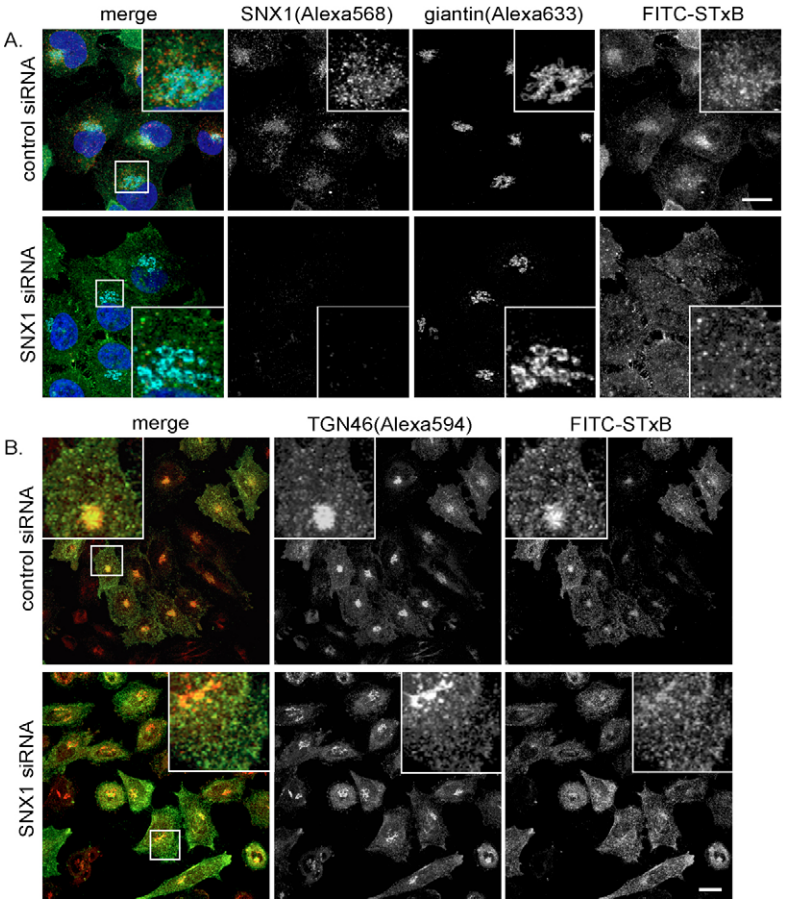

Fig. 4. SNX1-suppression does not grossly perturb Golgi complex and/or TGN appearance. (A,B) Control and SNX1-suppressed cells were subjected to toxin-uptake assay with FITC-STxB (green channel) for 30 minutes, and were then fixed and immunolabeled for either (A) SNX1 (Alexa594, red channel) and giantin (Alexa633, cyan channel) or (B) TGN46 (Alexa594, red channel). Bars, 20 μm.

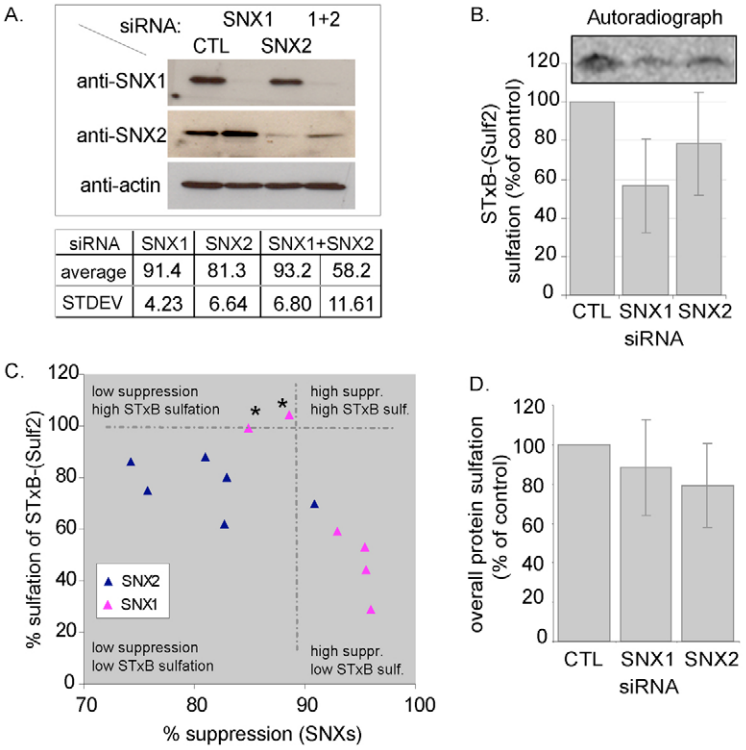

siRNA	SNX1	SNX2	SNX1+SNX2	
average	91.4	81.3	93.2	58.2
STDEV	4.23	6.64	6.80	11.61

Fig. 5. Analysis of STxB sulfation in SNX1- and SNX2-suppressed cells. The levels of TGN-localized STxB in control and SNX1- and SNX2-suppressed cells (individually and jointly) was quantified using a biochemical sulfation assay (see Materials and Methods and text for details). (A) Representative western blot showing levels of siRNA-mediated protein suppression. The table summarizes quantified levels of suppression achieved (ImageQuant) from $n \geqslant 4$ assays (n=6, for SNX1 and SNX2 individually). (B) The autoradiograph shows a typical result of a sulfation experiment using the B-($Sulf_2$) construct. The graph summarizes results from six independent sets (each in duplicates) as percent of control. Autoradiographs were quantified by densitometry and normalized to overall levels of protein sulfation. In SNX1-suppressed cells, sulfation was reduced by 43±24.4% compared with control cells, whereas in SNX2-suppressed cells sulfation was reduced by only 22±26.7%; values are given as the mean ± standard deviation (s.d.). (C) Levels of siRNA-mediated suppression as determined by western blotting and quantified by densitometry were plotted against the levels of STxB sulfation (each data point represents mean from duplicates, normalized to global sulfation) for six experimental sets (pink triangles, SNX1 siRNA; blue triangles, SNX2 siRNA). Lower levels of SNX1-suppression (<90%) do not result in reduced sulfation (asterisks). The regions were determined using the lowest suppression level for SNX1 (x-axis) not inducing a reduction in STxB sulfation (100%, y-axis). (D) Graph shows mean levels (± s.d.) of overall protein sulfation for the different siRNA conditions from at least five different experiments (in duplicates).

treated cells (Fig. 8C,D). Importantly, when we analyzed the kinetics of $Alexa^{555}$-CTxB transport from early endosomes to the Golgi complex, as determined from its colocalization with giantin (Fig. 8E), the trafficking of $Alexa^{555}$-CTxB was not reduced in SNX1-suppressed cells (27±13%) compared to control cells (13±6%) (Fig. 8F). Note that the degree of colocalization in SNX2-suppressed cells was similar to the degree measured for SNX1-suppressed and control cells (15±8%). These data therefore suggest that, at single-cell level, neither SNX1 nor SNX2 suppression reduces endosome-to-TGN transport of CTxB significantly and that, in contrast to STxB transport, retrograde transport of CTxB is less reliant upon SNX1.

Discussion

In the present study, combining single-cell fluorescent-toxin-uptake assays and well-established biochemical population-based analyses, we have established that RNAi-mediated silencing of SNX1 significantly perturbs retrograde endosome-to-TGN transport of the Shiga toxin B-subunit. We furthermore have shown that, in contrast to SNX1, the closely related SNX2 does not markedly alter the delivery of STxB to the TGN. Our data, together with evidence that RNAi-mediated suppression of the retromer component VPS26 also perturbs retrograde STxB transport (M.V.B. and P.J.C., unpublished data) (Popoff et al., 2007) showed that retrograde early-endosome-to-TGN transport of Shiga toxin occurs, at least in part, via a SNX1-regulated and/or retromer-regulated mechanism.

Perhaps surprisingly, given that Shiga and cholera toxins have been proposed to enter the Golgi complex via the same transport intermediates (Nichols et al., 2001) and both depend on syntaxin 5 and syntaxin 16 (Amessou et al., 2007), we presented evidence, based on fluorescent-toxin-uptake assays, that SNX1-suppression does not significantly reduce endosome-to-TGN transport of cholera toxin B-subunit. As far as we are aware, this is the first description of a molecular entity defining a retrograde pathway that differentially selects between these toxins. The questions how such differential sorting is achieved and whether this requires other components of the cargo-selective retromer subcomplex remain to be addressed.

Our study has also raised the issue of how the retromer complex relates to those other trafficking pathways that exist between the endosome and the TGN-Golgi complex. As it is clear that the retromer plays an important role in regulating endosome-to-TGN transport of the CI-MPR (Arighi et al., 2004; Carlton et al., 2004; Seaman, 2004), at least some components of the retromer transport machinery must be shared between CI-MPR and Shiga toxin trafficking. Indeed, a requirement for clathrin, epsinR and dynamin (Saint-Pol et al., 2004; Lauvrak et al., 2004) as well as lipid rafts (Falguieres et al., 2001; Carroll et al., 2001) are common features of both endosome-to-TGN transport of CI-MPR and Shiga toxin transport. Yet, although there is evidence that in order to efficiently transport Shiga toxin from endosomes to the TGN various components of the fusion machinery are required, such as Rab6A′ (Mallard et al., 2002; Del Nery et al., 2006), golgin-97 and tGolgin-1 (Lu et al., 2004; Yoshino et al., 2005), as well as syntaxin 5 and syntaxin 16 (Mallard et al., 2002; Tai et al., 2004; Amessou et al., 2007), there is so far no evidence to suggest a link between these components and the retromer sorting machinery. So, future studies are aimed at comparing the required molecular entities in more detail to establish whether these components act on successive steps or whether we are indeed looking at multiple paralleled pathways, as suggested by the incomplete block of transport to the TGN upon suppression of SNX1.

The question of how the retromer relates to these other retrograde transport pathways also arises when one considers endosome-to-TGN retrieval of the CI-MPR. Besides the retromer other proteins, including PACS1, in complex with the clathrin adaptors AP1 and GGA3 have been shown to be important in retrieval of the CI-MPR to the TGN (Wan et al., 1998; Meyer et al., 2000; Crump et al., 2001; Scott et al., 2003; Scott et al., 2006). Furthermore, there is evidence that the Rab9-TIP47 complex regulates retrieval of the CI-MPR from late endosomes back to the Golgi complex (Diaz and Pfeffer, 1998; Carroll et al., 2001; Barbero et al., 2002). So far, there is no evidence for a direct link between the retromer and any of these other CI-MPR retrieval pathways. Nevertheless, previous EM studies have strongly suggested that SNX1-positive and/or CI-MPR-positive tubular profiles originate from a portion of early-endosomal membrane that does not possess a recognizable electron-dense clathrin coat (Carlton et al., 2004). Conversely, clathrin and epsinR were both shown to be important for retrograde transport of the CI-MPR (Saint-Pol et al., 2004). This raises the question whether clathrin-dependent and retromer-dependent retrograde transport pathways exist as two distinct itineraries from the early endosome, or whether they function within the same pathway but at different stages – in other words – in a processive manner. This model is further supported by the finding that at ultrastructural level, unlike SNX1 (Carlton et al., 2004), VPS26 also localizes to some extent to the bilayered clathrin coat (Arighi et al., 2004). Moreover, clathrin and the retromer component VPS26 do not only colocalize on STxB-positive endosomes at EM level but, upon their suppression, STxB appears to be trapped in these distinct endosomal subdomains (Popoff et al., 2007). These findings underline a model in which clathrin and the retromer act at different stages on the same transport pathway.

Our finding that SNX2 only plays a minor role in STxB retrograde transport, whereas suppression of the two retromer components VPS26 and SNX1 produced major effects, adds to the controversy surrounding the potential role of SNX2 in retromer function. One of the many outstanding questions in mammalian retromer biology relates to the identity of the mammalian analog of yeast Vps17p. Whereas there seems to be no direct homolog in mammals, SNX2 has been argued to function as an equivalent to Vps17p (Haft et al., 2000; Rojas et al., 2007). Consistent with this, SNX2 can form heterodimers with SNX1 in a manner similar to Vps5p and Vps17p (Haft et al., 1998; Kurten et al., 2001; Seaman and Williams, 2002; Rojas et al., 2007). Further still, genetic studies in mice have even pointed to a more crucial role of SNX2 over SNX1 during embryonic development (Schwarz et al., 2002; Griffin et al., 2005), especially in combination with knocked out Vps26 (Griffin et al., 2005). Conversely, other data suggest that SNX2 does not interact with any other components of the retromer besides SNX1 (Gullapalli et al., 2004), and only mildly affects the kinetics of endosome-to-TGN delivery of the CI-MPR (Carlton et al., 2005). So, although it might appear that down-modulation was not efficient enough to reveal this effect, we were unable to establish a critical threshold for SNX2-suppression with regard to B-($Sulf_2$) sulfation. Even at the lowest examined suppression levels, sulfation never reached levels obtained in control levels. In assays less susceptible to potential effects of SNX2 suppression on the rate of proliferation (that furthermore allowed monitoring of suppression levels of individual cells) the toxin clearly accumulated at the TGN, which argues against a major role of this SNX in endosomal retention of the toxin and is in line with previous findings for the CI-MPR (Carlton et al., 2005; Rojas et al., 2007). In this context, it should also be noticed that, like suppression of SNX1, SNX2 suppression does not appear to affect retrograde CTxB transport. Interestingly, while preparing this manuscript, Skanland et al. reported that SNX2 but not SNX1 is important in retrograde transport of the plant toxin ricin (Skanland et al., 2007). Like Shiga and cholera toxins, ricin is an ER-trafficking toxin; but unlike STxB and CI-MPR, its endosome-to-TGN transport does not appear to depend on clathrin or Rab9 (Lombardi et al., 1993; Iversen et al., 2001; Lauvrak et al., 2004; Saint-Pol et al., 2004).

The finding that SNX2 and SNX1 appear to

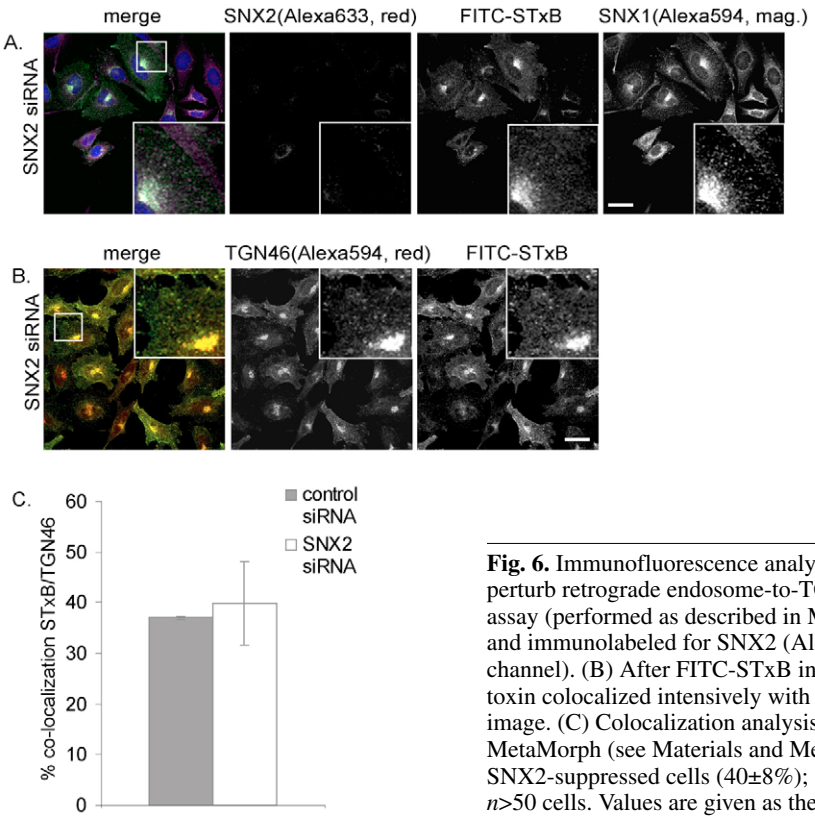

Fig. 6. Immunofluorescence analysis confirms that SNX2-suppression does not grossly perturb retrograde endosome-to-TGN transport of FITC-STxB. (A) FITC-STxB-uptake-assay (performed as described in Materials and Methods). Cells were fixed after 30 minutes and immunolabeled for SNX2 (Alexa633, red channel) and SNX1 (Alexa594, magenta channel). (B) After FITC-STxB internalization for 30 minutes in SNX2-suppressed cells, the toxin colocalized intensively with TGN46 (Alexa594, red channel); yellow in the merged image. (C) Colocalization analysis of STxB and TGN46 of confocal image sections using MetaMorph (see Materials and Methods for further details) in control cells (37±0.4%) and SNX2-suppressed cells (40±8%); s.d. determined from mean for individual visual fields for n>50 cells. Values are given as the mean ± standard deviation (s.d.); bars, 20 μm.

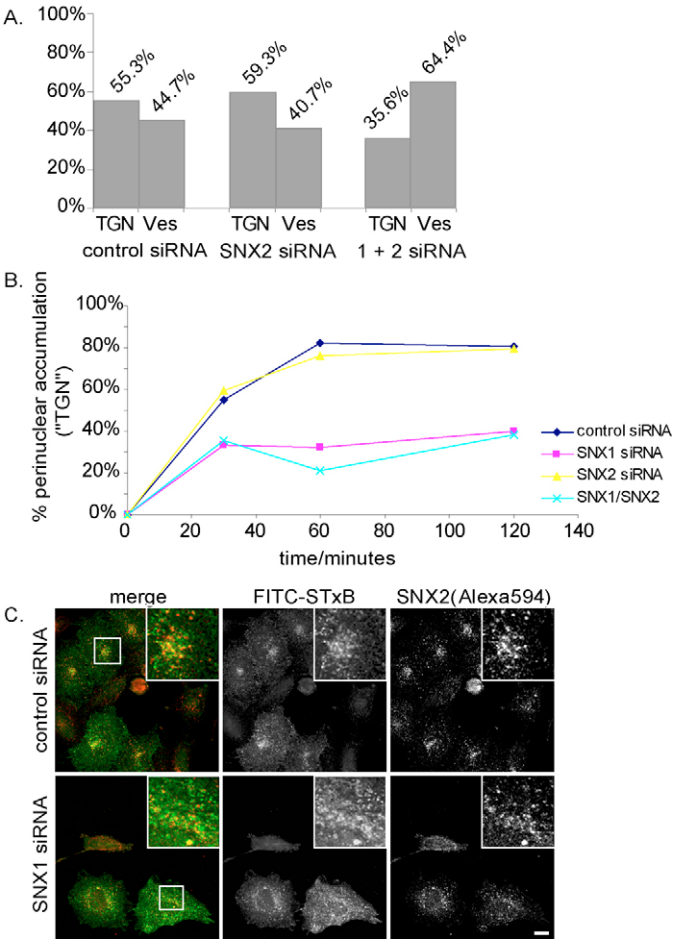

Fig. 7. Quantification of STxB localization in SNX2-suppressed cells and cells that were jointly suppressed for SNX1 and SNX2. (A) The assay was performed as described for Fig. 3 and the localization of FITC-STxB in >600 cells was scored after 30 minutes of toxin uptake, as described for Fig. 3. (B) Representative data set for TGN-like accumulation of FITC-STxB over time (n>600 for each sample; scored for 30, 60 and 120 minutes) for control cells and, SNX2-suppressed cells and cells that were jointly suppressed for SNX1 and SNX2. (C) SNX2 clustering in the perinuclear area is dependent on SNX1. Control and SNX1-suppressed cell were subjected to a FITC-STxB-uptake assay (green channel). The toxin was surface-bound at 4°C and internalized at 37°C for 30 minutes. Fixed cells were immunolabeled with anti-SNX2 antibody (Alexa633, red cannel). Bar, 10 μm.

have independent properties with regards to toxin traffic (Skanland et al., 2007) (and this study), but also with respect to receptor sorting (Gullapalli et al., 2004; Gullapalli et al., 2006), point towards a model in which SNX1 and SNX2 can function independently of each other and, at least for SNX1, independently of Vps26 (Gullapalli et al., 2006). In support of this model is the result from a recent RNAi loss-of-function screen that identified sorting nexins SNX5 and SNX6 as additional candidates for the retromer complex as their suppression induces a 'retromer-like phenotype' with regard to CI-MPR redistribution (Wassmer et al., 2006). Further still, the requirement for to suppress SNX1 by more than 92% in order to efficiently inhibit STxB sulfation, presented in this study, suggests the concept of a critical but minimal threshold level of SNX1 to maintain efficient transport towards the TGN. Importantly, SNX5 and SNX6 are crucial for SNX1 protein stability, because their suppression significantly decreased SNX1 protein levels (Wassmer et al., 2006). Analogously, binding of GFP-SNX5 to tubular membranes appears to crucially depend on SNX1 (Kerr et al., 2006). By contrast, the regulation of SNX1 and SNX2 protein levels is less striking. In this context, it is to note that we occasionally observed an upregulation of SNX2 in SNX1-suppressed cells, which might explain the weaker effect of SNX2 siRNA for the joint SNX1 and SNX2 suppression – despite the same protocol.

In conclusion, the fact that there is no direct mammalian homolog for yeast Vps17p but that other sorting nexins can induce a SNX1-suppression-like phenotype regarding CI-MPR traffic (Wassmer et al., 2006), suggests a model in which the mammalian retromer has evolved to a point where it can modify the composition of its membrane coat to allow different sorting nexins to control its function. Additionally, the SNX composition of the retromer complex might be cell type-dependent and, as suggested by the genetic studies (Schwarz et al., 2002; Griffin et al., 2005), the function of individual proteins, including SNX2, might differ during developmental stages.

Materials and Methods

Antibodies and reagents

Monoclonal anti-SNX1 and anti-SNX2 antibodies were purchased from BD Biosciences. Rabbit polyclonal anti-SNX1 antibody was a kind gift from Matthew Seaman, CIMR, UK. Generation of FITC-labeled Shiga toxin B-subunit (FITC-STxB), the B-($Sulf_2$) toxin subunit and the monoclonal anti-Shiga toxin antibody 13C4 has been described elsewhere (Johannes et al., 1997; Mallard et al., 1998). Polyclonal rabbit anti-giantin antibody was from Covance Research, the polyclonal sheep anti-TGN46 antibody was from Serotec. The monoclonal anti-actin antibody (clone AC-74) and the DAPI reagent were obtained from Sigma. All HRP-coupled secondary antibodies, ECL detection kits and films were purchased from GE Healthcare. All other secondary antibodies and Alexa Fluor-555-coupled CTxB ($Alexa^{555}$-CTxB) were obtained from Invitrogen. HeLa cells (CCL-2) were obtained from ATCC-LGC Promochem. All other reagents were obtained from SigmaAldrich or Invitrogen, if not stated otherwise.

RNA interference

The small interfering (siRNA) duplexes were purchased from Dharmacon (control target: AAGACAAGAACCAGAACGCCA; SNX1 target: AAGAACAAGACC-AAGAGCCAC; SNX2 target: AAGUCCAUCAUCUCCAGAACC). HeLa cells were seeded at a density of 0.95×10^5 cells per 35-mm well. On the following day, cells were transfected with 100 nM siRNA duplex using Oligofectamine according to the manufacturer's instructions. After 55 hours, cells were trypsinised and for every transfection condition, several wells containing 120,000 cells per 16-mm well were seeded. After further 13 hours, cells of one well per condition were harvested and lysed to assess the levels of SNX1 protein suppression by western blotting. Suppression efficiency was quantified by densitometry using ImageQuant software (GE Healthcare). The remainder of cells was used for toxin uptake assays and sulfation analyses.

Toxin-uptake assays

Toxin-uptake assays were essentially carried out as previously described (Mallard et al., 1998). In brief, cells were incubated with 1 μM FITC-STxB or $Alexa^{555}$-CTxB for 30 minutes at 4°C, washed three times with PBS to remove any unbound toxin, shifted to 37°C (in full DMEM) for indicated times and subsequently fixed using 4% para-formaldehyde (PFA) at room temperature (RT) or 37°C for 15 minutes.

Indirect immunofluorescence

Fixed cells were permeabilized for 5 minutes at RT using 0.1% Triton X-100 in PBS, and then transferred into PBS containing 1% BSA (1% P-BSA) for 30 minutes at RT to block unspecific binding. Cells were incubated with primary antibodies (see Materials and Methods) in 1% P-BSA for 1 hour. After three washes with 1% P-BSA, cells were incubated with the appropriate secondary antibodies (see Antibodies and reagents) in PBS for 1 hour. Cells were washed washed three times with PBS and then, where applicable, stained with DAPI for 10 minutes. After a

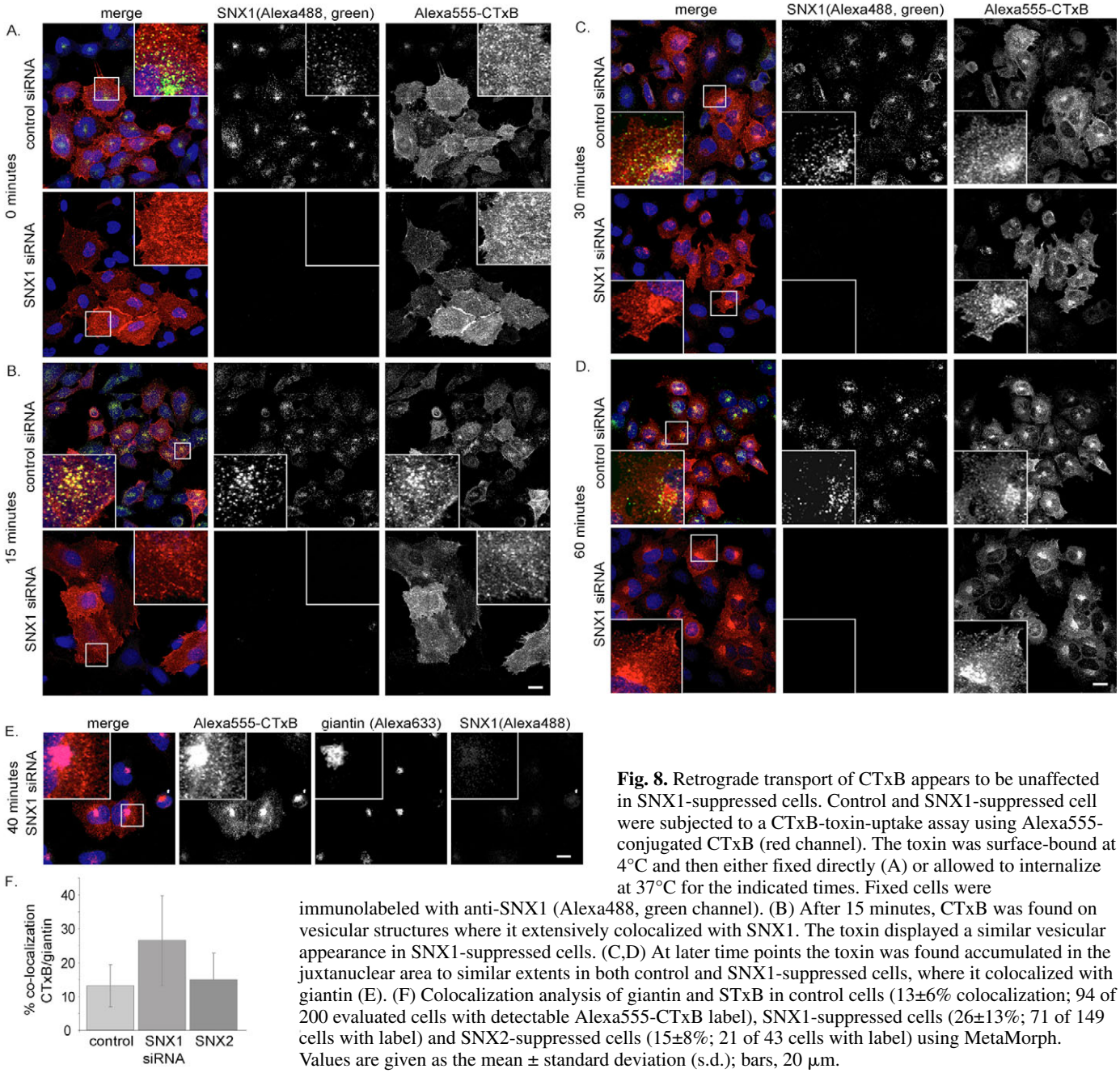

Fig. 8. Retrograde transport of CTxB appears to be unaffected in SNX1-suppressed cells. Control and SNX1-suppressed cell were subjected to a CTxB-toxin-uptake assay using Alexa555-conjugated CTxB (red channel). The toxin was surface-bound at 4°C and then either fixed directly (A) or allowed to internalize at 37°C for the indicated times. Fixed cells were immunolabeled with anti-SNX1 (Alexa488, green channel). (B) After 15 minutes, CTxB was found on vesicular structures where it extensively colocalized with SNX1. The toxin displayed a similar vesicular appearance in SNX1-suppressed cells. (C,D) At later time points the toxin was found accumulated in the juxtanuclear area to similar extents in both control and SNX1-suppressed cells, where it colocalized with giantin (E). (F) Colocalization analysis of giantin and STxB in control cells (13±6% colocalization; 94 of 200 evaluated cells with detectable Alexa555-CTxB label), SNX1-suppressed cells (26±13%; 71 of 149 cells with label) and SNX2-suppressed cells (15±8%; 21 of 43 cells with label) using MetaMorph. Values are given as the mean ± standard deviation (s.d.); bars, 20 μm.

brief rinse with H_2O, coverslips were mounted onto slides using Mowiol. Slides were analyzed by epifluorescence microscopy using a Leica DM LB2 upright fluorescence microscope or a Leica AOBS SP2 confocal imaging system, taking eight to ten optical slices. Images were merged using Leica software or ImageJ (NIH public domain software) and, where necessary, contrast and brightness for the entire image were adjusted using Adobe Photoshop.

Sulfation analysis

Sulfation analysis was essentially carried out as previously described (Mallard et al., 1998). Briefly, cells treated with siRNA as described, were starved for 2 hours in sulfate-free medium, before 1 μM of the modified B-($Sulf_2$) toxin subunit (per 120,000 cells) was surface-bound to cells at 4°C. After three washes, toxin uptake assay was performed using medium containing radioactively labeled [^{35}S]Na_2O_4 (GE Healthcare) for 20 minutes (0.5 mCi/ml). Cells were then lysed in RIPA buffer (1% NP40, 0.5% deoxycholate and 0.5% SDS in 1×PBS, supplemented with a protease inhibitor cocktail) and the toxin was immunoprecipitated (IP) using the 13C4 antibody and protein G-sepharose beads (GE Healthcare). Precipitates were subjected to gel electrophoresis and, after drying, gels were analyzed by autoradiography. In parallel, to assess the levels of global sulfation of cellular molecules, the proteins in the IP supernatants were precipitated using 100% trichloroacetic acid and filtrates were analyzed by gamma counting. To normalize the data, values obtained by gamma counting were multiplied with the data obtained by autoradiography and then divided by values obtained for control samples. For each set of experiments and condition, duplicate analyses were performed.

Colocalization analysis

To quantify the toxin distribution in control and SNX-suppressed cells after 30 minutes of FITC-STxB uptake (as described above), cells were additionally immunolabeled with TGN46 or giantin, and imaged under identical conditions using confocal microscopy, taking eight to ten optical slices per visual field. For several visual fields, yielding at least 50 cells per sample, colocalization was analyzed using MetaMorph software (Molecular Devices). Colocalization was determined for every optical section individually for one visual field at a time; from these values, the mean was calculated. The standard deviation (s.d.) gives the deviation between individual visual fields. To quantify colocalization between FITC-STxB and SNX1, the colocalization plug-in in ImageJ (NIH public domain software) was used.

Enumeration of vesicles was done using the Colony Counter tool of ImageQuant TL software (GE Healthcare) on individual and colocalization composite images obtained from the ImageJ analysis.

This work was funded by the Wellcome Trust and a Medical Research Council Infrastructure Award (G4500006), which established the School of Medical Sciences Cell Imaging Facility. We thank Mark Jepson and Alan Leard for their assistance. Work in the Traffic and Signaling Laboratory was supported by grants from the Ligue Nationale contre le Cancer and Association de Recherche contre le Cancer numbers 5177 and 3105. M.V.B. is supported by the Department of Biochemistry, University of Bristol, PerkinElmer Life and Analytical Sciences, and acknowledges the receipt of an EMBO Short Term Fellowship.

References

Amessou, M., Fradagada, A., Falguieres, T., Lord, J. M., Smith, D. C., Roberts, L. M., Lamaze, C. and Johannes, L. (2007). Syntaxin 16 and syntaxin 5 are required for efficient retrograde transport of several exogenous and endogenous cargo proteins. *J. Cell Sci.* **120**, 1457-1468.

Arighi, C. N., Hartnell, L. M., Aguilar, R. C., Haft, C. R. and Bonifacino, J. S. (2004). Role of the mammalian retromer in sorting of the cation-independent mannose 6-phosphate receptor. *J. Cell Biol.* **165**, 123-133.

Barbero, P., Bittova, L. and Pfeffer, S. R. (2002). Visualization of Rab9-mediated vesicle transport from endosomes to the trans-Golgi in living cells. *J. Cell Biol.* **156**, 511-518.

Bonifacino, J. S. and Rojas, R. (2006). Retrograde transport from endosomes to the *trans*-Golgi network. *Nat. Rev. Mol. Cell Biol.* **7**, 568-579.

Burda, P., Padilla, S. M., Sarkar, S. and Emr, S. D. (2002). Retromer function in endosome-to-Golgi retrograde transport, is regulated by the yeast Vps34 PtdIns 3-kinase. *J. Cell Sci.* **115**, 3889-3900.

Carlton, J. G., Bujny, M. V., Peter, B. J., Oorschot, V. M. J., Rutherford, A. C., Mellor, H., Klumperman, J., McMahon, H. T. and Cullen, P. J. (2004). Sorting nexin-1 mediates tubular endosome-to-TGN transport through co-incidence sensing of high curvature membranes and 3-phosphoinositides. *Curr. Biol.* **14**, 1791-1800.

Carlton, J. G., Bujny, M. V., Peter, B. J., Oorschot, V. M. J., Rutherford, A. C., Arkell, R. S., Klumperman, J., McMahon, H. T. and Cullen, P. J. (2005). Sorting nexin-2 is associated with tubular elements of the early endosome, but is not essential for retromer-mediated endosome-to-TGN transport. *J. Cell Sci.* **118**, 4527-4539.

Carroll, K. S., Hanna, J., Simon, I., Krise, J., Barbero, P. and Pfeffer, S. R. (2001). Role of Rab9 GTPase in facilitating receptor recruitment by TIP47. *Science* **292**, 1373-1376.

Crump, C. M., Xiang, Y., Thomas, L., Gu, F., Austin, C., Tooze, S. A. and Thomas, G. (2001). PACS-1 binding to adaptors is required for acidic cluster motif-mediated protein traffic. *EMBO J.* **20**, 2191-2201.

Del Nery, E., Miserey-Lenkei, S., Falguieres, T., Nizak, C., Johannes, L., Perez, F. and Goud, B. (2006). Rab6A and Rab6A′ GTPases play non-overlapping roles in membrane trafficking. *Traffic* **7**, 394-407.

Diaz, E. and Pfeffer, S. R. (1998). TIP47: a cargo selection device for mannose 6-phosphate receptor trafficking. *Cell* **93**, 433-443.

Falguieres, T., Mallard, F., Baron, C., Hanu, C., Lingwood, C., Goud, B., Salamero, J. and Johannes, L. (2001). Targeting of Shiga toxin B-subunit to retrograde transport route in association with detergent-resistant membranes. *Mol. Biol. Cell* **12**, 2453-2468.

Fishman, P. H., Moss, J. and Vaughan, M. (1976). Uptake and metabolism of gangliosides in transformed mouse fibroblasts. Relationship of ganglioside structure to choleragen response. *J. Biol. Chem.* **251**, 4490-4494.

Griffin, C. T., Trejo, J. and Magnuson, T. (2005). Genetic evidence for a mammalian retromer complex containing sorting nexins 1 and 2. *Proc. Natl. Acad. Sci. USA* **102**, 15173-15177.

Gullapalli, A., Garrett, T. A., Paing, M. M., Griffin, C. T., Yang, Y. and Trejo, J. (2004). A role for sorting nexin-2 in epidermal growth factor receptor down-regulation: evidence for distinct functions of sorting nexin-1 and -2 in protein trafficking. *Mol. Biol. Cell* **15**, 2143-2155.

Gullapalli, A., Wolfe, B. L., Griffin, C. T., Magnuson, T. and Trejo, J. (2006). An essential role for SNX1 in lysosomal sorting of protease-activated receptor-1: evidence for retromer-, Hrs-, and Tsg101-independent functions of sorting nexins. *Mol. Biol. Cell* **17**, 1228-1238.

Haft, C. R., de la Luz Sierra, M., Barr, V. A., Haft, D. H. and Taylor, S. I. (1998). Identification of a family of sorting nexin molecules and characterization of their association with receptors. *Mol. Cell. Biol.* **18**, 7278-7287.

Haft, C. R., de la Luz Sierra, M., Bafford, R., Lesniak, M. A., Barr, V. A. and Taylor, S. I. (2000). Human orthologues of yeast vacuolar protein sorting proteins Vps26, **29**, and **35**, assembly into multimeric complexes. *Mol. Biol. Cell* **11**, 4105-4116.

Iversen, T. G., Skretting, G., Llorente, A., Nicoziani, P., van Deurs, B. and Sandvig, K. (2001). Endosome to Golgi transport of ricin is independent of clathrin and of the Rab9-and Rab11-GTPases. *Mol. Biol. Cell* **12**, 2099-2107.

Iwaki, T., Hosomi, A., Tokudomi, S., Kusunoki, Y., Fujita, Y., Giga-Hama, Y., Tanaka, N. and Takegawa, K. (2006). Vacuolar protein sorting receptor in *Schizosaccharomyces pombe*. *Microbiology* **152**, 1523-1532.

Jacewicz, M., Clausen, H., Nudelman, E., Donohue-Rolfe, A. and Keusch, G. T. (1986). Pathogenesis of shigella diarrhea. XI. Isolation of a shigella toxin-binding glycolipid from rabbit jejunum and HeLa cells and its identification as globotriaosylceramide. *J. Exp. Med.* **163**, 1391-1404.

Jaillais, Y., Fobis-Loisy, I., Meige, C., Rollin, C. and Gaude, T. (2006). AtSNX1 defines an endosome for auxin-carrier trafficking in *Arabidopsis*. *Nature* **443**, 106-109.

Johannes, L. and Decaudin, D. (2005). Protein toxins: intracellular trafficking for targeted therapy. *Gene Ther.* **16**, 1360-1368.

Johannes, L., Tenza, D., Antony, C. and Goud, B. (1997). Retrograde transport of KDEL-bearing B-fragment of Shiga toxin. *J. Biol. Chem.* **272**, 19554-19561.

Kerr, M. C., Lindsay, M. R., Luetterforst, R., Hamilton, N., Simpson, F., Parton, R. G., Gleeson, P. A. and Teasdale, R. D. (2006). Visualisation of macropinosome maturation by the recruitment of sorting nexins. *J. Cell Sci.* **119**, 3967-3980.

Kurten, R. C., Cadena, D. L. and Gill, G. N. (1996). Enhanced degradation of EGF receptors by sorting nexin, SNX1. *Science* **272**, 1008-1010.

Kurten, R. C., Eddington, A. D., Chowdhury, P., Smith, R. D., Davidson, A. D. and Shank, B. B. (2001). Self-assembly and binding of a sorting nexin to sorting endosomes. *J. Cell Sci.* **114**, 1743-1756.

Lauvrak, S. U., Torgersen, M. L. and Sandvig, K. (2004). Efficient endosome-to-Golgi transport of Shiga toxin is dependent on dynamin and clathrin. *J. Cell Sci.* **117**, 2321-2331.

Lombardi, D., Soldati, T., Riederer, M. A., Goda, Y., Zerial, M. and Pfeffer, S. R. (1993). Rab9 functions in transport between late endosomes and the trans Golgi network. *EMBO J.* **12**, 677-682.

Lu, L., Tai, G. and Hong, W. (2004). Autoantigen Golgin-97, and effector of Arl1 GTPase, participates in traffic from the endosome to the TGN. *Mol. Biol. Cell* **15**, 4426-4443.

Mallard, F., Tenza, D., Antony, C., Salamero, J., Goud, B. and Johannes, L. (1998). Direct pathway from early/recycling endosomes to the Golgi apparatus revealed through the study of Shiga toxin B-fragment transport. *J. Cell Biol.* **143**, 973-990.

Mallard, F., Tang, B. L., Galli, T., Tenza, D., Saint-Pol, A., Yue, X., Antony, C., Hong, W. J., Goud, B. and Johannes, L. (2002). Early/recycling endosomes-to-TGN transport involves two SNARE complexes and Rab6 isoform. *J. Cell Biol.* **156**, 653-664.

Meyer, C., Zizioli, D., Lausmann, S., Eskelinen, E. L., Hamann, J., Saftig, P., van Figura, K. and Schu, P. (2000). μ1A-adaptin-deficient mice: lethality, loss of AP-1 binding and rerouting of mannose 6-phosphate receptors. *EMBO J.* **19**, 2193-2203.

Nichols, B. J., Kenworthy, A. K., Polishchuk, R. S., Lodge, R., Roberts, T. H., Hirschberg, K., Phair, R. D. and Lippincott-Schwartz, J. (2001). Rapid cycling of lipid raft markers between the cell surface and Golgi complex. *J. Cell Biol.* **153**, 529-541.

Niehrs, C. and Huttner, W. B. (1990). Purification and characterization of tyrosylprotein sulfotransferase. *EMBO J.* **9**, 35-42.

Nothwehr, S. F., Ha, S. A. and Bruinsma, P. (2000). Sorting of yeast membrane proteins into an endosome-to-Golgi pathway involves direct interaction of their cytosolic dmains with Vps35p. *J. Cell Biol.* **151**, 297-309.

Oliviusson, P., Heinzerling, O., Hillmer, S., Hinz, G., Tse, Y. C., Jiang, L. and Robinson, D. G. (2006). Plant retromer, localized to the prevacuolar compartment and microvesicles in *Arabidopsis*, may interact with vacuolar sorting receptors. *Plant Cell* **18**, 1239-1252.

Popoff, V., Mardones, G. A., Tenza, D., Rojas, R., Lamaze, C., Bonifacino, J. S., Raposo, G. and Johannes, L. (2007). The retromer complex and clathrin define an early endosomal retrograde exit site. *J. Cell Sci.* **120**, 2022-2031.

Prasad, B. C. and Clark, S. G. (2006). Wnt signaling establishes anteroposterior neuronal polarity and requires retromer in C. elegans. *Development* **133**, 1757-1766.

Reddy, J. V. and Seaman, M. N. J. (2001). Vps26p, a component of the retromer, directs the interactions of Vps35p in endosome-to-Golgi retrieval. *Mol. Biol. Cell* **12**, 3242-3256.

Rojas, R., Kametaka, S., Haft, C. R. and Bonifacino, J. S. (2007). Interchangeable but essential functions of SNX1 and SNX2 in the association of retromer with endosomes and the trafficking of mannose 6-phosphate receptors. *Mol. Cell. Biol.* **27**, 1112-1124.

Saint-Pol, A., Yelamos, B., Amessou, M., Mills, I. G., Dugast, M., Tenza, D., Schu, P., Antony, C., McMahon, H. T., Lamaze, C. et al. (2004). Clathrin adaptor espinR is required for retrograde sorting on early endosomal membranes. *Dev. Cell* **6**, 525-538.

Sandvig, K. and van Deurs, B. (2002). Membrane traffic exploited by protein toxins. *Annu. Rev. Cell Dev. Biol.* **18**, 1-24.

Sandvig, K. and van Deurs, B. (2005). Delivery into cells: lessons learned from plant and bacterial toxins. *Gene Ther.* **12**, 865-872.

Schwarz, D. G., Griffin, C. T., Schneider, E. A., Yee, D. and Magnuson, T. (2002). Genetic analysis of sorting nexins 1 and 2 reveals a redundant and essential function in mice. *Mol. Biol. Cell.* **13**, 3588-3600.

Scott, G. K., Gu, F., Crump, C. M., Thomas, L., Wan, L., Xiang, Y. and Thomas, G. (2003). The phosphorylation state of an autoregulatory domain controls PACS-1-directed protein traffic. *EMBO J.* **22**, 6234-6244.

Scott, G. K., Fei, H., Thomas, L., Medigeshi, G. R. and Thomas, G. (2006). A PACS-1, GGA3 and CK2 complex regulates CI-MPR trafficking. *EMBO J.* **25**, 4423-4435.

Seaman, M. N. J. (2004). Cargo-selective endosomal sorting for retrieval to the Golgi requires retromer. *J. Cell Biol.* **165**, 111-122.

Seaman, M. N. J. (2005). Recycle your receptors with retromer. *Trends Cell Biol.* **15**, 68-75.

Seaman, M. N. J. and Williams, H. P. (2002). Identification of the functional domains of yeast sorting nexins Vps5p and Vps17p. *Mol. Biol. Cell* **13**, 2826-2840.

Seaman, M. N. J., Marcusson, E. G., Cereghino, J. L. and Emr, S. D. (1997). Endosome

to Golgi retrieval of the vacuolar protein sorting receptor, Vps10p, requires the function of the VPS29, VPS30, and VPS35 gene products. *J. Cell Biol.* **137**, 79-92.

Seaman, M. N. J., McCaffrey, J. M. and Emr, S. D. (1998). A membrane coat complex essential for endosome-to-Golgi retrograde transport in yeast. *J. Cell Biol.* **142**, 665-681.

Shimada, T., Koumoto, Y., Li, L., Yamazaki, M., Kondo, M., Nishimura, M. and Hara-Mishimura, I. (2006). AtVPS29, a putative component of the retromer complex, is required for the efficient sorting of seed storage proteins. *Plant Cell Physiol.* **47**, 1187-1194.

Skanland, S. S., Wälchli, S., Utskarpen, A., Wandinger-Ness, A. and Sandvig, K. (2007). Phosphoinositide-regulated retrograde transport of ricin: crosstalk between hVps34 and sorting nexins. *Traffic* **8**, 297-309.

Spooner, R. A., Smith, D. C., Easton, A. J., Roberts, L. M. and Lord, J. M. (2006). Retrograde transport pathways utilized by viruses and protein toxins. *Virol. J.* **3**, 26.

Tai, G., Lu, L., Wang, T. L., Tang, B. L., Goud, B., Johannes, L. and Hong, W. (2004). Participation of the syntaxin5/Ykt6/GS28/GS15 SNARE complex in transport from the early/recycling endosome to the trans-Golgi network. *Mol. Biol. Cell* **15**, 4011-4022.

Wan, L., Molloy, S. S., Thomas, L., Liu, G., Xiang, Y., Rybak, S. L. and Thomas, G. (1998). PACS-1 defines a novel gene family of cytosolic sorting proteins required for *trans*-Golgi network localization. *Cell* **94**, 205-216.

Wassmer, T., Attar, N., Bujny, M. V., Oakley, J., Traer, C. J. and Cullen, P. J. (2006). A loss-of-function screen reveals sorting nexin-5 and sorting nexin-6 as potential components of the mammalian retromer. *J. Cell Sci.* **120**, 45-54.

Yoshino, A., Setty, S. R. G., Poynton, C., Whiteman, E. L., Saint-Pol, A., Burd, C. G., Johannes, L., Holzbaur, E. L., Koval, M., McCaffrey, J. M. et al. (2005). tGolgi-1 (p230, golgin-245) modulates Shiga-toxin transport to the Golgi and Golgi motility towards the microtubule-organizing centre. *J. Cell Sci.* **118**, 2279-2293.

Journal of Cell Science